



1 **Feasibility analysis of using inverse modeling for estimating field-scale evapotranspiration in**
2 **maize and soybean fields from soil water content monitoring networks**

3

4 Foad Foolad¹, Trenton E. Franz², Tiejun Wang^{2,3}, Justin Gibson², Ayse Kilic^{1,2}, Richard G. Allen⁴,
5 Andrew Suyker²

6

7 ¹Civil Engineering Department, University of Nebraska-Lincoln, USA

8 ²School of Natural Resources, University of Nebraska-Lincoln, USA

9 ³Institute of Surface-Earth System Science, Tianjin University, P.R. China

10 ⁴Kimberly Research and Extension Center, University of Idaho, USA

11

12 **Keywords:** Evapotranspiration; soil water content; inverse modeling; soil hydraulic parameters;

13 Cosmic ray neutron probe

14 Corresponding author T.E. Franz (tfranz2@unl.edu)

15

16

17

18



19 **Abstract**

20 In this study the feasibility of using inverse vadose zone modeling for estimating field scale actual
21 evapotranspiration (ET_a) was explored at a long-term agricultural monitoring site in eastern
22 Nebraska. Data from both point scale soil water content sensors (SWC) and the area-average
23 technique of cosmic-ray neutron probes were evaluated against independent ET_a estimates from a
24 co-located eddy covariance tower. While this methodology has been successfully used for estimates
25 of groundwater recharge it was critical to assess the performance of other components of the water
26 balance such as ET_a . In light of the recent evaluation of Land Surface Model (LSM) performance
27 from the plumber experiment, independent estimates of hydrologic state variables and fluxes are
28 critically needed benchmarks. The results here indicate reasonable estimates of daily and annual ET_a
29 from the point sensors but with highly varied soil hydraulic function parameterizations due to local
30 soil texture variability. The results of multiple soil hydraulic parameterizations leading to equally
31 good ET_a estimates is consistent with the hydrological principle of equifinality. While this study
32 focused on one particular site the framework can be easily applied to other SWC monitoring
33 networks across the globe. The value added products of groundwater recharge and ET_a flux from the
34 SWC monitoring networks will provide additional and more robust benchmarks for the validation of
35 LSM that continue to improve their forecast skill. In addition, the value added products of
36 groundwater recharge and ET_a often have more direct impacts on societal decision making than SWC
37 alone. Water flux impacts human decision making from policies on the long-term management of
38 groundwater resources (recharge), to yield forecasts (ET_a), and to optimal irrigation scheduling (ET_a).
39 Illustrating the societal benefits of SWC monitoring is critical to insure the continued operation and
40 expansion of these public datasets.

41



42 1. Introduction

43 Evapotranspiration (ET) is an important component in terrestrial water and surface energy
44 balance. In the United States, ET comprises about 75% of annual precipitation, while in arid and
45 semiarid regions ET comprises more than 90% of annual precipitation (Zhang et al., 2001; Glenn et
46 al., 2007; Wang et al., 2009a). As such, an accurate estimation of ET is critical in order to predict
47 changes in hydrological cycles and improve water resource management (Suyker et al., 2008;
48 Anayah and Kaluarachchi, 2014). Given the importance of ET , an array of measurement techniques
49 at different temporal and spatial scales have been developed (c.f., Maidment, 1992; Zhang et al.,
50 2014), including lysimeter, Bowen ratio, Eddy-Covariance (EC), and satellite-based surface energy
51 balance approaches. However, simple, low-cost, and accurate field-scale measurements of actual ET
52 (ET_a) still remain a challenge due to the uncertainties of available estimation techniques (Wolf et al.,
53 2008; Li et al., 2009; Senay et al., 2011; Stoy, 2012). For instance, field techniques, such as EC and
54 Bowen ratio, can provide relatively accurate estimation of local ET_a , but are often cost prohibitive
55 for wide-spread use beyond research applications (Baldocchi et al., 2001; Irmak, 2010). By
56 comparison, satellite-based remote sensing techniques are far less costly for widespread spatial
57 coverage (Allen et al., 2007), but are limited by their accuracy, temporal sampling frequency (e.g.,
58 Landsat 8 has a 16-day overpass), and technical issues that further limit temporal sampling periods
59 (e.g., cloud coverage during overpass) (Chemin and Alexandridis, 2001; Xie et al., 2008; Li et al.,
60 2009; Kjaersgaard et al., 2012).

61 As a complement to the above mentioned techniques, recent studies have used process-based
62 vadose zone models (VZMs) for estimating field-scale ET_a with reasonable success, particularly in
63 arid and semi-arid areas (Twarakavi et al., 2008; Izadifar and Elshorbagy, 2010; Galleguillos et al.,
64 2011; Wang et al., 2016). Although VZMs are time and cost effective for estimating field-scale ET_a ,



65 they generally require complex model parameterizations and inputs, some of which are not readily
66 available (e.g., soil hydraulic parameters and plant physiological parameters; Wang et al., 2016). In
67 order to address the issue of missing soil hydraulic parameters, a common approach is to use
68 pedotransfer functions to convert readily available soil information (e.g., texture, bulk density, etc.)
69 to soil hydraulic parameters (Wösten et al., 2001); however, significant uncertainties are usually
70 associated with this method for estimating local scale water fluxes (Wang et al., 2015). In fact,
71 Nearing et al. (2016) identified soil hydraulic property estimation as the largest source of information
72 lost when evaluating different land surface modeling schemes versus a soil moisture benchmark.
73 Poor and uncertain parameterization of soil hydraulic properties are a clear weakness of land surface
74 models (LSMs) predictive skill in sensible and latent heat fluxes (Best et al., 2015). This problem
75 will continue to compound with the continuing spatial refinement of hyper-resolution LSMs grid
76 cells to less than 1 km (Wood et al., 2011).

77 In order to address the challenge of field scale estimation of soil hydraulic properties, here
78 we utilize inverse modeling for estimating soil hydraulic parameters based on field measurements
79 of soil water content (*SWC*) (c.f. Hopmans and Šimunek, 1999; Ritter et al., 2003). While VZM-
80 based inverse modeling approaches have already been examined for estimating groundwater
81 recharge (e.g., Jiménez-Martínez et al., 2009; Andreasen et al., 2013; Min et al., 2015; Ries et al.,
82 2015; Turkeltaub et al., 2015; Wang et al., 2016), its application for ET_a estimation has not been
83 adequately tested. Moreover, we note that simultaneous estimation of *SWC* states and surface energy
84 fluxes within LSMs is complicated by boundary conditions, model parameterization, and model
85 structure (Nearing et al., 2016). With the incorporation of regional soil datasets in LSMs like Polaris
86 (Chaney et al., 2016), effective strategies for estimating ground truth soil hydraulic properties from



87 existing *SWC* monitoring networks (e.g., SCAN, CRN, COSMOS, State/National Mesonets, c.f. Xia
88 et al. (2015)) will become critical for continuing to improve the predictive skill of LSMs.

89 The aim of this study is to examine the feasibility of using inverse VZM modeling for
90 estimating field scale ET_a based on long-term local meteorological and *SWC* observations for an
91 Ameriflux (Baldocchi et al., 2001) eddy covariance site in eastern Nebraska, USA. The remainder
92 of the paper is organized as follows. In the methods section we will describe the widely used VZM,
93 Hydrus-1D (Simunek et al., 2013), used to obtain soil hydraulic parameters. We will assess the
94 feasibility of using both profiles of in-situ *SWC* probes as well as the area-average *SWC* technique
95 from Cosmic-Ray Neutron Probes (CRNP). In the results section we will compare the calibrated
96 VZM with independent ET_a estimates provided by EC observations. Finally, we note that while this
97 study focused on one particular study site in eastern Nebraska, the methodology can be easily
98 adapted to a variety of *SWC* monitoring networks across the globe (Xia et al., 2015).

99

100 **2. Materials and Methodology**

101 **2.1 Study Site**

102 The study site is located in eastern Nebraska, USA at the University of Nebraska Agricultural
103 and Development Center near Mead. The field site (US-Ne3, Figure 1a, 41.1797° N°, 96.4397° W)
104 is part of the Ameriflux Network (Baldocchi et al., 2001) and has been operating continually since
105 2001. The regional climate is of a continental semiarid type with a mean annual precipitation of 784
106 mm/year (According to the Ameriflux US-Ne3 website). According to the Web Soil Survey Data
107 (Soil Survey Staff, 2016), the soils at the site are comprised mostly of silt loam and silty clay loam.
108 Soybean and maize are rotationally grown at the site under rainfed conditions, with the growing



109 season beginning in early May and ending in October (Kalfas et al., 2011). Since 2001, crop
110 management practices (i.e., planting density, cultivars, irrigation, and herbicide and pesticide
111 applications) have been applied in accordance with standard best management practices prescribed
112 for production-scale maize systems (Suyker et al., 2008). More detailed information about site
113 conditions can be found in Suyker et al. (2004) and Verma et al. (2005).

114 An EC tower was constructed at the center of the field (Figure 1 and Figure 2a), which
115 continuously measures water, energy, and CO₂ fluxes (e.g., Baldocchi et al., 1988). In this study,
116 hourly latent heat flux measurements were integrated to daily values and then used for calculating
117 daily ET_a integrated over the field scale. Detailed information on the EC measurements and
118 calculation procedures for ET_a are given in Suyker and Verma (2009). Hourly air temperature,
119 relative humidity, horizontal wind speed, net radiation, and precipitation were also measured at the
120 site. Destructive measurements of leaf area index (LAI) were made every 10 to 14 days during the
121 growing season at the study site (Suyker et al., 2005). We note that the LAI data were linearly
122 interpolated to provide daily estimates. Theta probes (Delta-T Devices, Cambridge, UK) were
123 installed at 4 locations in the study field with measurement depths of 10, 25, 50, and 100 cm at each
124 location to monitor hourly SWC in the root zone (Suyker et al., 2008). Here, we denote these four
125 locations as TP 1 (41.1775° N, 96.4442° W), TP 2 (41.1775° N, 96.4428° W), TP 3 (41.1775° N,
126 96.4402° W), and TP 4 (41.1821° N, 96.4419° W) (Figure 1b). Daily precipitation (P) and reference
127 evapotranspiration (ET_r) computed for the tall (alfalfa) reference crop using the ASCE standardized
128 Penman-Monteith equation (ASCE-EWRI 2005) are shown in Figure 3 for the study period (2007–
129 2012) at the study site.

130 In addition, a Cosmos-Ray Neutron Probe (CRNP, model CRS 2000/B, HydroInnova LLC,
131 Albuquerque, NM, USA) (41.1798 N°, 96.4412° W) was installed near the EC tower (Figure 1b and



132 2b) on 20 April 2011. The CRNP measures hourly moderated neutron counts (Zreda et al., 2008,
133 2012), which are converted into *SWC* following standard correction procedures and calibration
134 methods (c.f., Zreda et al., 2012). In addition, the changes in above-ground biomass were removed
135 from the CRNP estimates of *SWC* following Franz et al. (2015). The CRNP measurement depth
136 (Franz et al., 2012) at the site varies between 15-40 cm, depending on *SWC*. Note for simplicity in
137 this analysis we assume the CRNP has an effective depth of 20 cm (mean depth of 10 cm) for all
138 observational periods. For a more general integration of CRNP data into the NOAH LSM data
139 assimilation framework, we refer to the work of Shuttleworth et al. (2013) and Rosolem et al. (2014).
140 The areal footprint of the CRNP is $\sim 250 \pm 50$ m radius circle (see Desilets and Zreda (2013) and
141 Kohli et al. (2015) for details). Here we assume for simplicity the EC and CRNP footprints are both
142 representative of the areal-average field conditions.

143

144 **2.2. Model setup**

145 **2.2.1 Vadose Zone Model**

146 The Hydrus-1D model (Šimunek et al., 2013), which is based on the Richards equation, was
147 used to calculate ET_a . The setup of the Hydrus-1D model is explained in details by Jiménez-Martínez
148 et al. (2009), Min et al. (2015), and Wang et al. (2016), and only a brief description of the model
149 setup is provided here. Given the measurement depths of the Theta Probes, the simulated soil profile
150 length was chosen to be 175 cm with 176 nodes at 1 cm intervals. An atmospheric boundary
151 condition with surface runoff was selected as the upper boundary. This allowed the occurrence of
152 surface runoff when precipitation rates were higher than soil infiltration capacity or if the soil
153 became saturated. According to a nearby USGS monitoring well (Saunders County, NE, USGS



154 411005096281502, ~2.7 km away), the depth to water tables was greater than 12 m during the study
155 period. Therefore, free drainage was used as the lower boundary condition.

156 Daily ET_r was calculated using the ASCE Penman-Monteith equation for the tall (0.5 m)
157 ASCE reference (ASCE-EWRI, 2005), and daily potential evapotranspiration (ET_p) was calculated
158 according to FAO 56 (Allen et al., 1998):

$$159 \quad ET_p(t) = K_c(t) \times ET_r(t) \quad (1)$$

160 where K_c is a crop-specific coefficient at time t . The estimates of growth stage lengths and K_c values
161 for maize and soybean suggested by Allen et al. (1998) and Min et al. (2015) were adopted in this
162 study. In order to partition daily ET_p into potential transpiration (T_p) and potential evaporation (E_p)
163 Beer's law was used as follows:

$$164 \quad E_p(t) = ET_p(t) \times e^{-k \times LAI(t)} \quad (2)$$

$$165 \quad T_p(t) = ET_p(t) - E_p(t) \quad (3)$$

166 where k is an extinction coefficient with a value set to 0.5 (Wang et al., 2009b) and LAI (L^2/L^2) is leaf
167 area index described above. The root water uptake, which was assumed to be equal to actual
168 transpiration, was simulated according to the Feddes model, based on T_p and root density distribution
169 (Feddes et al., 1978). Since the study site has annual cultivation rotations between soybean and
170 maize, the root growth model from the Hybrid-Maize Model (Yang et al., 2004) was used to model
171 the root growth during the growing season:



$$\left. \begin{array}{l}
 \text{if } D < MRD \\
 D = \frac{AGDD}{GDD_{Silking}} MRD \\
 \\
 \text{else} \\
 \\
 D = MRD
 \end{array} \right\} \quad (4)$$

173 Where D (cm) is plant root depth for each growing season day, MRD is the maximum root depth
 174 (assumed equal to 150 cm for maize and 120 cm for soybean in this study following Yang et al.
 175 (2004)), $AGDD$ is the accumulated growing degree days, and $GDD_{Silking}$ is the accumulated GDD at
 176 the silking point (e.g., Accumulated plant GDD approximately 60-70 days after crop emergence).
 177 GDD for each growing season day was calculated as:

$$178 \quad GDD = \frac{T_{max} - T_{min}}{2} - T_{base} \quad (5)$$

179 where T_{max} and T_{min} are the maximum and minimum daily temperature ($^{\circ}C$), respectively, and T_{base}
 180 is the base temperature set to be $10^{\circ}C$ following McMaster and Wilhelm (1997) and Yang et al.
 181 (1997).

182

183 2.2.2 Inverse modeling to estimate soil hydraulic parameters

184 Inverse modeling was used to estimate soil hydraulic parameters for the van Genuchten-
 185 Mualem model (Mualem, 1976; van Genuchten, 1980):

$$186 \quad \theta(h) = \begin{cases} \theta_r + \frac{\theta_s - \theta_r}{(1 + |\alpha h|^n)^m}, & h < 0 \\ \theta_s, & h \geq 0 \end{cases} \quad (6)$$



$$187 \quad K(S_e) = K_s \times S_e^l \times [1 - (1 - S_e^{1/m})^m]^2 \quad (7)$$

188

189 where θ (L^3/L^3) is volumetric *SWC*; θ_r (L^3/L^3) and θ_s (L^3/L^3) are residual and saturated moisture
 190 content, respectively; h (L) is pressure head; K (L/T) and K_s (L/T) are unsaturated and saturated
 191 hydraulic conductivity, respectively; and $S_e (= (\theta - \theta_r) / (\theta_s - \theta_r))$ (-) is saturation degree. With respect to
 192 the fitting factors, α (1/L) is inversely related to air entry pressure, n (-) measures the pore size
 193 distribution of a soil with $m = 1 - 1/n$, and l (-) is a parameter accounting for pore tortuosity and
 194 connectivity.

195 Daily *SWC* data from the four TP locations and CRNP location were used for the inverse
 196 modeling. Based on the measurement depths of the TPs, the simulated soil columns were divided
 197 into four layers (i.e., 0-15 cm, 15-35 cm, 35-75 cm, and 75-175 cm), which led to a total of 24
 198 hydraulic parameters to be optimized (θ_r , θ_s , α , n , K_s , and L). In order to efficiently optimize the
 199 parameters, we used the method outlined in Turkeltaub et al. (2015). Specifically, the van Genuchten
 200 parameters of the upper two layers were first optimized, while the parameters of the lower two layers
 201 were fixed, since water contents of the lower layers changed more slowly and over a smaller range
 202 than the upper layers. Then, the optimized van Genuchten parameters of the upper two layers were
 203 kept fixed, while the parameters of the lower two layers were optimized. The process was continued
 204 until there were no further improvements in the optimized hydraulic parameters or until the changes
 205 in the lowest sum of squares were less than 0.1%. Given the sensitivity of the optimization results
 206 to the initial guesses of soil hydraulic parameters in the Hydrus model, soil hydraulic parameters
 207 from six soil textures were used as initial inputs for the optimizations at each location (Carsel and
 208 Parish, 1988), including sandy clay loam, silty clay loam, loam, silt loam, silt, and clay loam. Based
 209 on the length of available *SWC* data from the TP measurements, the periods of 2007, 2008-2010,



210 and 2011-2012 were used as the spin-up, calibration, and validation periods, respectively. Moreover,
211 to minimize the impacts of freezing conditions on *SWC* measurements, data from January to March
212 of each calendar year were removed (based on available soil temperature data) from the
213 optimizations.

214 In addition to the TP profile observations, we used the CRNP area-average *SWC* in the
215 inverse procedure to develop an independent set of soil parameters. The CRNP was assumed to
216 provide *SWC* data with an average effective measurement depth of 20 cm at this study site. The
217 observation point was therefore set at 10 cm. In addition, soil properties were assumed to be
218 homogeneous throughout the simulated soil column with a length of 175 cm. Since the CRNP was
219 installed in 2011 at the study site, the periods of 2011, 2012-2013, and 2014 were used as spin-up,
220 calibration, and validation periods, respectively, for the optimization procedure.

221 The lower and upper bounds on the van Genuchten parameters used are given in Table 1.
222 With respect to the goodness-of-fit assessment, four performance criteria were selected to evaluate
223 the model results, including R-squared (R^2), Mean Average Error (MAE), Root Mean Square Error
224 (RMSE), and the Nash-Sutcliffe Efficiency (NSE):

$$225 \quad MAE = \frac{1}{n} \sum_{i=1}^n |P_i - O_i| \quad (8)$$

$$226 \quad RMSE = \sqrt{\frac{1}{n} \sum_{i=1}^n (P_i - O_i)^2} \quad (9)$$

$$227 \quad NSE = 1 - \frac{\sum_{i=1}^n (P_i - O_i)^2}{\sum_{i=1}^n (O_i - \bar{O})^2} \quad (10)$$

228 where n is the total number of *SWC* data points, O_i , and P_i are respectively the observed and
229 simulated daily *SWC* on day i , and \bar{O} is the observed mean value. Finally, based on the best scores



230 (i.e., lowest MAE and RMSE, and highest NSE scores), the best optimized soil parameter values at
231 each location were selected. Using the selected parameters, the Hydrus model was run in a forward
232 mode in order to estimate ET_a between 2007 and 2012. We note 2004-2006 was used as a spin-up
233 period for the forward model.

234

235 **3. Results and Discussions**

236 **3.1 Inverse Vadose Zone Modeling Results**

237 The time series of the average SWC from the four TP locations along with one standard
238 deviation at each depth is plotted in Figure 4. Despite the small spatial scale in this study (~65 ha),
239 Figure 4 clearly shows that SWC varies considerably across the site, particularly during the growing
240 season. The comparison between SWC data from the CRNP and spatial average of SWC data at four
241 TP locations in the study field (*i.e.* average of 10 and 25 cm depths at each location) is presented in
242 Figure 5 and 6. The daily RMSE between the spatial average of the TPs and CRNP data is 0.037
243 cm^3/cm^3 , which is consistent with other studies that reported similar values in semiarid shrublands
244 (Franz et al., 2012), German Forests (Bogena et al., 2013, Baatz et al., 2014), montane forests in
245 Utah (Lv et al., 2014), sites across Australia (Hawdon et al., 2014), and a mixed land use agricultural
246 site in Austria (Franz et al. 2016). Note we would expect lower RMSE ($\sim < 0.02 \text{ cm}^3/\text{cm}^3$) with
247 additional point sensors located at shallower depths and in more locations spatially. Never-the-less,
248 the consistent behavior between the spatial mean SWC of TPs and the CRNP allows us to explore
249 spatial variability of soil hydraulic properties within footprint using inverse modeling. This will be
250 described in the next sections. The study period (2007-2012, Figure 7) contained significant
251 interannual variability in precipitation. During the spin-up period in 2007, the annual precipitation



252 (942 mm) was higher than the mean annual precipitation (784 mm), 2008 was a wet year (997 mm),
253 2009–2011 were near average years (715 mm), and 2012 was a record dry year (427 mm) with a
254 widespread drought across the region. Therefore, both wet and dry years were considered in the
255 inverse modeling simulation period.

256 As an illustration, Figure 8 shows the daily observed and simulated *SWC* during the
257 calibration (2008–2010) and validation (2011–2012) periods at the TP 1 location (the simulation
258 results of the other three sites can be found in the supplemental Figures S1, S2, and S3). The results
259 of four performance criteria (e.g., R^2 , MAE, RMSE, and NSE) between simulated and observed
260 *SWC* data at TPs and CRNP locations are presented in Tables 2 and 3.

261 Similar to previous studies (e.g., Jiménez-Martínez et al., 2009; Andreasen et al., 2013; Min
262 et al., 2015; Wang et al., 2016), the results of all the performance criteria at TPs locations show the
263 capability of inverse modeling in estimation of soil hydraulic parameters. The results of the
264 calibration period (2008–2010) indicate that the simulated and observed *SWC* values are in good
265 agreement throughout the whole period. However, the match between the simulated and observed
266 *SWC* are better in the shallower depths of 10 and 25 cm (Figure 8 and Table 2). In addition, the
267 simulated and observed data were well matched during the validation period (2011–2012), except
268 during the second half of 2012 when the extreme drought occurred. Reasons for this disagreement
269 in the observed and simulated *SWC* data will be discussed in the following sections.

270 The results of inverse modeling using the CRNP data indicate the feasibility of using these
271 data to estimate effective soil hydraulic parameters (Table 3). Based on the performance criteria
272 (Table 3), the simulated data are fairly well-matched with the observed *SWC* data during both the
273 calibration and validation periods. However, as the crops extracted water from deeper soil layers



274 and due to the fact that the CRNP observational depth is limited to near surface layers (~20 cm), it
275 is clear from the data that the comparison between the simulated and observed values deteriorates
276 over the growing season (Figure 9). The results suggest that it might be more appropriate to use the
277 CRNP data for inverse modeling during periods that are dominated by soil evaporation (Jana et al.,
278 2016) and/or for sites with shallow rooted vegetation only. Additional information from deeper soil
279 probes or more complex modeling approaches such as data assimilation techniques (Rosolem et al.,
280 2014, Renzullo et al., 2014) may be needed to fully utilize the CRNP data for the entire growing
281 season; however, this is beyond the scope of this study and future investigations are still needed.

282 Table 4 summarizes the optimized van Genuchten parameters for the four different depths
283 of the four TP locations and the single layer for the CRNP location. The optimized parameters were
284 then used to estimate ET_a for the entire study period as an independent comparison to the EC ET_a
285 data. The results of the ET_a evaluation will be discussed in the next section. According to the
286 simulation results (Table 4), in most of the soil layers, the TP 4 location possesses lower n , K_s , and
287 higher θ_r values than the other 3 locations (TPs 1-3), suggesting either underlying soil texture
288 variability in the field or texture dependent sensor sensitivity/calibration. As a validation for the
289 simulation results, the publicly available Web Soil Survey Data were used to explore whether the
290 optimized van Genuchten parameters from the inverse modeling (Figure 10 and Table 5) agreed with
291 the survey data. Based on the Web Soil Survey Data, the soil at the TP 4 location contains higher
292 clay percentage than the other locations. Meanwhile, the optimized parameters reflect the spatial
293 pattern of soil texture in the field as shown by the Web Soil Survey data (e.g., lower n and K_s values
294 and higher θ_r values at the TP 4 location with finer soil texture). Physically, finer-textured soils
295 generally have lower K_s and higher θ_r values (Carsel and Parrish, 1988). Moreover, the shape factor
296 n is indicative of pore size distributions of soils. In general, finer soils with smaller pore sizes tend



297 to have lower n values (Carsel and Parrish, 1988). The observed SWC at the TP 4 location is
298 consistently higher than the average SWC of the other three locations (Figure S4 in supplemental
299 materials), which can be partly attributed to the higher θ_r values at the TP 4 location (Wang and
300 Franz, 2015). Overall, the obtained van Genuchten parameters from the inverse modeling are in
301 good agreement with the spatial distribution of soil texture in the study field, indicating the capability
302 of using inverse VZM modeling to infer soil hydraulic properties.

303

304 **3.2 Comparison of modeled ET_a with observed ET_a**

305 Using the best fit soil hydraulic parameters for the four TP sites and the CRNP site, the
306 Hydrus-1D model was run in a forward mode to calculate ET_a over the entire study period. The
307 simulated daily ET_a was then compared with the independent EC ET_a measurements using the same
308 four performance criteria that were used to evaluate the simulated SWC time series (Table 6). The
309 performance criteria results indicate that the simulated daily ET_a is in a better agreement with EC
310 ET_a measurements at the TP 1-3 locations than at the TP 4 and CRNP locations (Table 6 and Figure
311 11). However, based on the performance criteria from inverse modeling results and based on the
312 Web Soil Survey Data, one can conclude that partly due to the spatial heterogeneity of soil texture
313 in the study field, spatial variation in ET_a rates likely exist over the field (e.g., less ET_a occurs at the
314 TP 4 location than from the other part of the field). In addition, higher surface runoff can be expected
315 at the TP 4 location due to finer-textured soils and therefore less stored water to support ET_a .
316 According to the simulation results the average surface runoff at the TP 4 location was about 44.8
317 mm/year from 2007 to 2012, while the average surface runoff at the other three locations (TPs 1-3)
318 was around 10.6 mm/year.



319 Given that CRNPs have a limited observational depth and only one single soil layer was
320 optimized in the inverse model for the CRNP, one could expect the simulated daily ET_a from the
321 CRNP to have larger uncertainty (e.g., RMSE of 1.26 mm/day at the CRNP location versus mean
322 RMSE value of 1.07 mm/day at TP locations). However, when the optimized soil parameters
323 obtained from the CRNP data were used to estimate ET_a , the model did simulate daily ET_a fairly
324 well during non-growing and early growing seasons in comparison to the EC ET_a measurements;
325 however, with the development of deeper root systems after mid-June, the simulation results of daily
326 ET_a did slightly deteriorate (Figure 13).

327 On the annual scale, ET_a measured by the EC tower accounted for 87% of annual P recorded
328 at the site during the study period (Figure 7). Overall, the simulated annual ET_a at all the TP and
329 CRNP locations is comparable to the annual ET_a measured by the EC tower, except during 2012
330 (Table 7, Figure 12 and Figure 13), in which a severe drought occurred in the region. One
331 explanation is that the plants extract more water from deeper layers under extreme drought
332 conditions than what we defined as a maximum rooting depth (150 cm for maize and 120 cm for
333 soybean) for the model, thus limiting the VZM model's ability to estimate ET_a accurately during the
334 drought year (2012). Given the fact that EC ET_a estimation can have up to 20% uncertainty
335 (Massman and Lee, 2002, and Hollineger and Richardson, 2005), and accounting for the natural
336 spatial variability of ET_a due to soil texture, the various ET_a estimation techniques performed well.
337 In fact, it is difficult to identify which is the clear solution if any. These results are consistent with
338 the concept of equifinality in hydrologic modeling given the complexity of natural systems (Beven
339 and Freer, 2001). Moreover, the findings here are consistent with Nearing et al. (2016) that show
340 information lost in model parameters greatly affects the soil moisture comparisons against a
341 benchmark. However, soil parameterization was less important in the loss of information for the



342 comparisons of ET /latent energy against a benchmark. Fully resolving these issues remains a key
343 challenge to the land surface modeling community and the model's ability to make accurate
344 predictions (Best 2015).

345

346 **4. Conclusions**

347 In this study the feasibility of using inverse vadose zone modeling for field scale ET_a
348 estimation was explored at an agricultural site in eastern Nebraska. Both point SWC sensors (TP)
349 and area-average techniques (CRNP) were explored. This methodology has been successfully used
350 for estimates of groundwater recharge but it was critical to assess the performance of other
351 components of the water balance such as ET_a . The results indicate reasonable estimates of daily and
352 annual ET_a but with varied soil hydraulic function parameterizations. The varied soil hydraulic
353 parameters were expected given the heterogeneity of soil texture at the site and consistent with the
354 principle of equifinality in hydrologic systems. We note that while this study focused on one
355 particular site, the framework can be easily applied to other networks of SWC monitoring across the
356 globe (Xia et al., 2015). The value added products of groundwater recharge and ET_a flux from the
357 SWC monitoring networks will provide additional and more robust benchmarks for the validation of
358 LSM that continue to improve their forecast skill.

359

360 **Acknowledgments**

361 This research is supported financially by the Daugherty Water for Food Global Institute at
362 the University of Nebraska, NSF EPSCoR FIRST Award, the Cold Regions Research Engineering
363 Laboratory through the Great Plains CESU, and an USGS104b grant. We sincerely appreciate the



364 support and the use of facilities and equipment provided by the Center for Advanced Land
365 Management Information Technologies, School of Natural Resources and data from Carbon
366 Sequestration Program, the University of Nebraska-Lincoln. TEF would like to thank Eric Wood for
367 his inspiring research and teaching career. No doubt the skills TEF learned while at Princeton in
368 formal course work, seminars, and discussions with Eric will serve him well in his own career.



369 **References**

- 370 Allen, R. G., Pereira, L. S., Raes, D., & Smith, M. (1998). Crop evapotranspiration-guidelines for
371 computing crop water requirements-FAO irrigation and drainage paper 56. FAO, Rome,
372 300(9), D05109.
- 373 Allen, R. G., Tasumi, M., & Trezza, R. (2007). Satellite-based energy balance for mapping
374 evapotranspiration with internalized calibration (METRIC)—Model. *Journal of Irrigation and*
375 *Drainage Engineering*, 133(4), 380-394.
- 376 Anayah, F. M., & Kaluarachchi, J. J. (2014). Improving the complementary methods to estimate
377 evapotranspiration under diverse climatic and physical conditions. *Hydrology and Earth*
378 *System Sciences*, 18(6), 2049-2064.
- 379 Andreasen, M., Andreasen, L. A., Jensen, K. H., Sonnenborg, T. O., & Bircher, S. (2013).
380 Estimation of regional groundwater recharge using data from a distributed soil moisture
381 network. *Vadose Zone Journal*, 12(3)
- 382 ASCE – EWRI. (2005). The ASCE Standardized reference evapotranspiration equation. ASCE-
383 EWRI Standardization of Reference Evapotranspiration Task Comm. Report, ASCE
384 Bookstore, ISBN 078440805, Stock Number 40805, 216 pages.
- 385 Baatz, R., Bogen, H., Franssen, H. H., Huisman, J., Qu, W., Montzka, C., et al. (2014).
386 Calibration of a catchment scale cosmic-ray probe network: A comparison of three
387 parameterization methods. *Journal of Hydrology*, 516, 231-244.
- 388 Baldocchi, D. D., Hincks, B. B., & Meyers, T. P. (1988). Measuring biosphere-atmosphere
389 exchanges of biologically related gases with micrometeorological methods. *Ecology*, 1331-
390 1340.
- 391 Baldocchi, D., Falge, E., Gu, L., & Olson, R. (2001). FLUXNET: A new tool to study the temporal
392 and spatial variability of ecosystem-scale carbon dioxide, water vapor, and energy flux
393 densities. *Bulletin of the American Meteorological Society*, 82(11), 2415.



- 394 Best, M., Abramowitz, G., Johnson, H., Pitman, A., Balsamo, G., Boone, A., et al. (2015). The
395 plumbing of land surface models: Benchmarking model performance. *Journal of*
396 *Hydrometeorology*, 16(3), 1425-1442.
- 397 Beven, K., & Freer, J. (2001). Equifinality, data assimilation, and uncertainty estimation in
398 mechanistic modelling of complex environmental systems using the GLUE methodology.
399 *Journal of Hydrology*, 249(1), 11-29.
- 400 Bogaen, H., Huisman, J., Baatz, R., Hendricks Franssen, H., & Vereecken, H. (2013). Accuracy of
401 the cosmic-ray soil water content probe in humid forest ecosystems: The worst case scenario.
402 *Water Resources Research*, 49(9), 5778-5791.
- 403 Carsel, R. F., & Parrish, R. S. (1988). Developing joint probability distributions of soil water
404 retention characteristics. *Water Resources Research*, 24(5), 755-769.
- 405 Chaney, N. W., Wood, E. F., McBratney, A. B., Hempel, J. W., Nauman, T. W., Brungard, C. W.,
406 et al. (2016). POLARIS: A 30-meter probabilistic soil series map of the contiguous United
407 States. *Geoderma*, 274, 54-67.
- 408 Chemin, Y., & Alexandridis, T. (2001). Improving spatial resolution of ET seasonal for irrigated
409 rice in Zhanghe, china. Paper Presented at the 22nd Asian Conference on Remote Sensing, 5.
410 pp. 9.
- 411 Desilets, D., & Zreda, M. (2013). Footprint diameter for a cosmic-ray soil moisture probe: Theory
412 and monte carlo simulations. *Water Resources Research*, 49(6), 3566-3575.
- 413 Feddes, R. A., Kowalik, P. J., & Zaradny, H. (1978). Simulation of field water use and crop yield.
414 Centre for Agricultural Publishing and Documentation.
- 415 Franz, T. E., Wahbi, A., Vreugdenhil, M., Weltin, G., Heng, L., Oismueller, M., et al. (2016).
416 Using cosmic-ray neutron probes to monitor landscape scale soil water content in mixed land
417 use agricultural systems. *Applied and Environmental Soil Science*, 2016



- 418 Franz, T. E., Wang, T., Avery, W., Finkenbiner, C., & Brocca, L. (2015). Combined analysis of
419 soil moisture measurements from roving and fixed cosmic ray neutron probes for multiscale
420 real-time monitoring. *Geophysical Research Letters*, 42(9), 3389-3396.
- 421 Franz, T. E., Zreda, M., Ferre, T., Rosolem, R., Zweck, C., Stillman, S., et al. (2012).
422 Measurement depth of the cosmic ray soil moisture probe affected by hydrogen from various
423 sources. *Water Resources Research*, 48(8)
- 424 Galleguillos, M., Jacob, F., Prévot, L., Lagacherie, P., & Liang, S. (2011). Mapping daily
425 evapotranspiration over a Mediterranean vineyard watershed. *Geoscience and Remote
426 Sensing Letters, IEEE*, 8(1), 168-172.
- 427 Glenn, E. P., Huete, A. R., Nagler, P. L., Hirschboeck, K. K., & Brown, P. (2007). Integrating
428 remote sensing and ground methods to estimate evapotranspiration. *Critical Reviews in Plant
429 Sciences*, 26(3), 139-168.
- 430 Hawdon, A., McJannet, D., & Wallace, J. (2014). Calibration and correction procedures for
431 cosmic-ray neutron soil moisture probes located across Australia. *Water Resources Research*,
432 50(6), 5029-5043.
- 433 Hollinger, D. Y., & Richardson, A. D. (2005). Uncertainty in eddy covariance measurements and
434 its application to physiological models. *Tree Physiology*, 25(7), 873-885.
- 435 Hopmans, J.W., Šimunek, J., 1999. Review of inverse estimation of soil hydraulic properties. In:
436 van Genuchten, M.Th. Leij, F.J., Wu, L. (Eds.), *Proceedings of the International Workshop
437 Characterization and Measurement of Hydraulic Properties of Unsaturated Porous Media*.
438 University of California, Riverside, 643–659. Irmak, S. (2010). Nebraska water and energy
439 flux measurement, modeling, and research network (NEBFLUX). *Transactions of the
440 ASABE*, 53(4), 1097-1115. Irmak, S. (2010). Nebraska water and energy flux measurement,
441 modeling, and research network (NEBFLUX). *Transactions of the ASABE*, 53(4), 1097-1115.



- 442 Izadifar, Z., & Elshorbagy, A. (2010). Prediction of hourly actual evapotranspiration using neural
443 networks, genetic programming, and statistical models. *Hydrological Processes*, 24(23), 3413-
444 3425.
- 445 Jana, R. B., Ershadi, A., & McCabe, M. F. Examining the relationship between intermediate scale
446 soil moisture and terrestrial evaporation within a semi-arid grassland.
- 447 Jiménez-Martínez, J., Skaggs, T., Van Genuchten, M. T., & Candela, L. (2009). A root zone
448 modelling approach to estimating groundwater recharge from irrigated areas. *Journal of*
449 *Hydrology*, 367(1), 138-149.
- 450 Kalfas, J. L., Xiao, X., Vanegas, D. X., Verma, S. B., & Suyker, A. E. (2011). Modeling gross
451 primary production of irrigated and rain-fed maize using MODIS imagery and CO₂ flux
452 tower data. *Agricultural and Forest Meteorology*, 151(12), 1514-1528.
- 453 Kjaersgaard, J., Allen, R., Trezza, R., Robinson, C., Oliveira, A., Dhungel, R., et al. (2012). Filling
454 satellite image cloud gaps to create complete images of evapotranspiration. *IAHS-AISH*
455 *Publication*, 102-105.
- 456 Köhli, M., Schrön, M., Zreda, M., Schmidt, U., Dietrich, P., & Zacharias, S. (2015). Footprint
457 characteristics revised for field-scale soil moisture monitoring with cosmic-ray neutrons.
458 *Water Resources Research*, 51(7), 5772-5790.
- 459 Li, Z., Tang, R., Wan, Z., Bi, Y., Zhou, C., Tang, B., et al. (2009). A review of current
460 methodologies for regional evapotranspiration estimation from remotely sensed data. *Sensors*,
461 9(5), 3801-3853.
- 462 Lv, L., Franz, T. E., Robinson, D. A., & Jones, S. B. (2014). Measured and modeled soil moisture
463 compared with cosmic-ray neutron probe estimates in a mixed forest. *Vadose Zone Journal*,
464 13(12)
- 465 Maidment, D. R. (1992). *Handbook of hydrology*. McGraw-Hill Inc.



- 466 Massman, W., & Lee, X. (2002). Eddy covariance flux corrections and uncertainties in long-term
467 studies of carbon and energy exchanges. *Agricultural and Forest Meteorology*, 113(1), 121-
468 144.
- 469 McMaster, G. S., & Wilhelm, W. (1997). Growing degree-days: One equation, two interpretations.
470 *Agricultural and Forest Meteorology*, 87(4), 291-300.
- 471 Min, L., Shen, Y., & Pei, H. (2015). Estimating groundwater recharge using deep vadose zone data
472 under typical irrigated cropland in the piedmont region of the north china plain. *Journal of*
473 *Hydrology*, 527, 305-315.
- 474 Mualem, Y. (1976). A new model for predicting the hydraulic conductivity of unsaturated porous
475 media. *Water Resources Research*, 12(3), 513-522.
- 476 Nearing, G. S., Mocko, D. M., Peters-Lidard, C. D., Kumar, S. V., & Xia, Y. (2016).
477 Benchmarking NLDAS-2 soil moisture and evapotranspiration to separate uncertainty
478 contributions. *Journal of Hydrometeorology*, 17(3), 745-759.
- 479 Renzullo, L. J., Van Dijk, A., Perraud, J., Collins, D., Henderson, B., Jin, H., et al. (2014).
480 Continental satellite soil moisture data assimilation improves root-zone moisture analysis for
481 water resources assessment. *Journal of Hydrology*, 519, 2747-2762.
- 482 Ries, F., Lange, J., Schmidt, S., Puhlmann, H., & Sauter, M. (2015). Recharge estimation and soil
483 moisture dynamics in a Mediterranean, semi-arid karst region. *Hydrology and Earth System*
484 *Sciences*, 19(3), 1439-1456.
- 485 Ritter, A., Hupet, F., Muñoz-Carpena, R., Lambot, S., & Vanclooster, M. (2003). Using inverse
486 methods for estimating soil hydraulic properties from field data as an alternative to direct
487 methods. *Agricultural Water Management*, 59(2), 77-96.
- 488 Rosolem, R., Hoar, T., Arellano, A., Anderson, J., Shuttleworth, W. J., Zeng, X., et al. (2014).
489 Translating aboveground cosmic-ray neutron intensity to high-frequency soil moisture
490 profiles at sub-kilometer scale. *Hydrology and Earth System Sciences*, 18(11), 4363-4379.



- 491 Schaap, M. G., Leij, F. J., & Van Genuchten, M. T. (2001). Rosetta: A computer program for
492 estimating soil hydraulic parameters with hierarchical pedotransfer functions. *Journal of*
493 *Hydrology*, 251(3), 163-176.
- 494 Senay, G. B., Budde, M. E., & Verdin, J. P. (2011). Enhancing the simplified surface energy
495 balance (SSEB) approach for estimating landscape ET: Validation with the METRIC model.
496 *Agricultural Water Management*, 98(4), 606-618.
- 497 Shuttleworth, J., Rosolem, R., Zreda, M., & Franz, T. (2013). The COsmic-ray soil moisture
498 interaction code (COSMIC) for use in data assimilation. *Hydrology and Earth System*
499 *Sciences*, 17(8), 3205-3217.
- 500 Šimunek, J., Šejna, M., Saito, H., Sakai, M., van Genuchten, M.T. (2013). The HYDRUS-1D
501 Software Package for Simulating the One-Dimensional Movement of Water, Heat, and Multiple
502 Solutes in Variably-Saturated Media, Version 4.17. Department of Environmental Sciences,
503 University of California Riverside, Riverside, California, USA, 307 pp.
- 504 Soil Survey Staff, Natural Resources Conservation Service, United States Department of Agriculture.
505 Web Soil Survey. Available online at <http://websoilsurvey.nrcs.usda.gov/>. Accessed in July,
506 2016.
- 507 Stoy, P. (2012). Evapotranspiration and energy flux observations from a global tower network with
508 a critical analysis of uncertainties. AGU Fall Meeting Abstracts, 1. pp. 06.
- 509 Suyker, A., Verma, S., Burba, G., Arkebauer, T., Walters, D., & Hubbard, K. (2004). Growing
510 season carbon dioxide exchange in irrigated and rainfed maize. *Agricultural and Forest*
511 *Meteorology*, 124(1), 1-13.
- 512 Suyker, A. E., & Verma, S. B. (2008). Interannual water vapor and energy exchange in an irrigated
513 maize-based agroecosystem. *Agricultural and Forest Meteorology*, 148(3), 417-427.
- 514 Suyker, A. E., & Verma, S. B. (2009). Evapotranspiration of irrigated and rainfed maize-
515 cropping systems. *Agricultural and Forest Meteorology*, 149(3), 443-452.



- 516 Suyker, A. E., Verma, S. B., Burba, G. G., & Arkebauer, T. J. (2005). Gross primary production
517 and ecosystem respiration of irrigated maize and irrigated soybean during a growing season.
518 *Agricultural and Forest Meteorology*, 131(3), 180-190.
- 519 Suyker, A. E., Verma, S. B., Burba, G. G., & Arkebauer, T. J. (2005). Gross primary production
520 and ecosystem respiration of irrigated maize and irrigated soybean during a growing season.
521 *Agricultural and Forest Meteorology*, 131(3), 180-190.
- 522 Turkeltaub, T., Kurtzman, D., Bel, G., & Dahan, O. (2015). Examination of groundwater recharge
523 with a calibrated/validated flow model of the deep vadose zone. *Journal of Hydrology*, 522,
524 618-627.
- 525 Twarakavi, N. K. C., Šimůnek, J., & Seo, S. (2008). Evaluating interactions between groundwater
526 and vadose zone using the HYDRUS-based flow package for MODFLOW. *Vadose Zone*
527 *Journal*, 7(2), 757-768.
- 528 van Genuchten, M. T. (1980). A closed-form equation for predicting the hydraulic conductivity of
529 unsaturated soils. *Soil Science Society of America Journal*, 44(5), 892-898.
- 530 Verma, S. B., Dobermann, A., Cassman, K. G., Walters, D. T., Knops, J. M., Arkebauer, T. J., et
531 al. (2005). Annual carbon dioxide exchange in irrigated and rainfed maize-based
532 agroecosystems. *Agricultural and Forest Meteorology*, 131(1), 77-96.
- 533 Wang, T., & Franz, T. E. (2015). Field observations of regional controls of soil hydraulic
534 properties on soil moisture spatial variability in different climate zones. *Vadose Zone Journal*,
535 14(8)
- 536 Wang, T., Franz, T. E., Yue, W., Szilagyi, J., Zlotnik, V. A., You, J., et al. (2016). Feasibility
537 analysis of using inverse modeling for estimating natural groundwater recharge from a large-
538 scale soil moisture monitoring network. *Journal of Hydrology*, 533, 250-265.
- 539 Wang, T., Franz, T. E., & Zlotnik, V. A. (2015). Controls of soil hydraulic characteristics on
540 modeling groundwater recharge under different climatic conditions. *Journal of Hydrology*,
541 521, 470-481.



- 542 Wang, T., Istanbuluoglu, E., Lenters, J., & Scott, D. (2009a). On the role of groundwater and soil
543 texture in the regional water balance: An investigation of the Nebraska sand hills, USA. *Water*
544 *Resources Research*, 45(10)
- 545 Wang, T., Zlotnik, V. A., Šimunek, J., & Schaap, M. G. (2009b). Using pedotransfer functions in
546 vadose zone models for estimating groundwater recharge in semiarid regions. *Water*
547 *Resources Research*, 45(4)
- 548 Wolf, A., Saliendra, N., Akshalov, K., Johnson, D. A., & Laca, E. (2008). Effects of different eddy
549 covariance correction schemes on energy balance closure and comparisons with the modified
550 bowen ratio system. *Agricultural and Forest Meteorology*, 148(6), 942-952.
- 551 Wood, E. F., Roundy, J. K., Troy, T. J., Van Beek, L., Bierkens, M. F., Blyth, E., et al. (2011).
552 Hyperresolution global land surface modeling: Meeting a grand challenge for monitoring
553 earth's terrestrial water. *Water Resources Research*, 47(5)
- 554 Wösten, J., Pachepsky, Y. A., & Rawls, W. (2001). Pedotransfer functions: Bridging the gap
555 between available basic soil data and missing soil hydraulic characteristics. *Journal of*
556 *Hydrology*, 251(3), 123-150.
- 557 Xia, Y., Ek, M. B., Wu, Y., Ford, T., & Quiring, S. M. (2015). Comparison of NLDAS-2
558 simulated and NASMD observed daily soil moisture. part I: Comparison and analysis. *Journal*
559 *of Hydrometeorology*, 16(5), 1962-1980.
- 560 Xie, Y., Sha, Z., & Yu, M. (2008). Remote sensing imagery in vegetation mapping: A review.
561 *Journal of Plant Ecology*, 1(1), 9-23.
- 562 Yang, H., Dobermann, A., Cassman, K. G., & Walters, D. T. (2004). Hybrid-maize. A Simulation
563 Model for Corn Growth and Yield. Nebraska Cooperative Extension CD, 9
- 564 Yang, W., Yang, L., & Merchant, J. (1997). An assessment of AVHRR/NDVI-ecoclimatological
565 relations in Nebraska, USA. *International Journal of Remote Sensing*, 18(10), 2161-2180.



- 566 Zhang, L., Dawes, W., & Walker, G. (2001). Response of mean annual evapotranspiration to
567 vegetation changes at catchment scale. *Water Resources Research*, 37(3), 701-708.
- 568 Zhang, Z., Tian, F., Hu, H., & Yang, P. (2014). A comparison of methods for determining field
569 evapotranspiration: Photosynthesis system, sap flow, and eddy covariance. *Hydrology and*
570 *Earth System Sciences*, 18(3), 1053-1072.
- 571 Zreda, M., Shuttleworth, W., Zeng, X., Zweck, C., Desilets, D., Franz, T., et al. (2012). COSMOS:
572 The cosmic-ray soil moisture observing system. *Hydrology and Earth System Sciences*,
573 16(11), 4079-4099.
- 574 Zreda, M., Desilets, D., Ferré, T., & Scott, R. L. (2008). Measuring soil moisture content non-
575 invasively at intermediate spatial scale using cosmic-ray neutrons. *Geophysical Research*
576 *Letters*, 35(21).
- 577



578 **List of Figures**

579 Figure 1. Study site (Mead Rainfed/US-Ne3) location in Nebraska (a) and locations of Eddy-
580 Covariance Tower (EC), Cosmic-Ray Neutron Probe (CRNP) and Theta Probes (TPs) at the
581 study site, 2014 (b).

582 Figure 2. Eddy-Covariance Tower (a) and Cosmic-Ray Neutron Probe (b) Located at the Mead
583 Rainfed (US-Ne3) Site.

584 Figure 3. Daily precipitation (P) and reference evapotranspiration (ET_r) during the calibration
585 (2008–2010) and validation (2011–2012) periods at the Mead Rainfed (US-Ne3) Site.

586 Figure 4. Annual precipitation (P) and annual actual evapotranspiration (ET_a) at the Mead Rainfed
587 (US-Ne3) Site.

588 Figure 5. Time series of daily CRNP and spatial average TP $SWC(\theta)$ data.

589 Figure 6. Comparison between daily CRNP and spatial average TP $SWC(\theta)$ data.

590 Figure 7. Temporal evolution of daily $SWC(\theta)$ at different soil depths. The black lines represent
591 daily mean $SWC(\theta)$ calculated from TPs in 4 different locations at study site and the blue areas
592 indicate one standard deviation.

593 Figure 8. Daily observed and simulated $SWC(\theta)$ during the calibration (2008–2010) and validation
594 (2011–2012) periods at TP 1 location.

595 Figure 9. Daily observed and simulated $SWC(\theta)$ during the calibration (2012–2013) and validation
596 (2014) periods at the location of Cosmic-Ray Neutron probe.

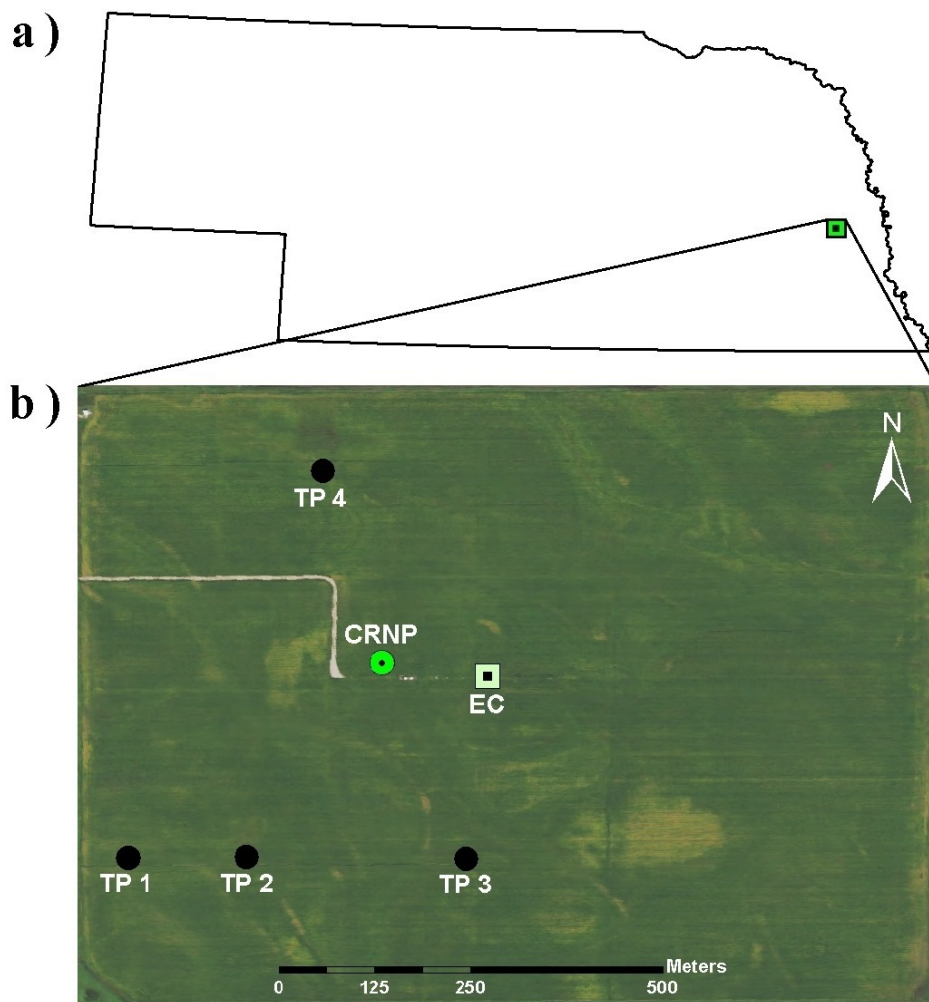


597 Figure 10. Variability of soil texture in the study field based on Web Soil Survey data (available at
598 <http://websoilsurvey.sc.egov.usda.gov/App/HomePage.htm>).

599 Figure 11. Annual actual Evapotranspiration (ET_a) estimation in different location at the study site
600 (2007-2012).

601 Figure 12. Mean Annual Actual Evapotranspiration (ET_a) estimation in different location at the
602 study site (2007-2012).

603 Figure 13. Cumulative simulated actual ET versus cumulative observed actual ET in different
604 locations at the study site (2007-2012).



605

606

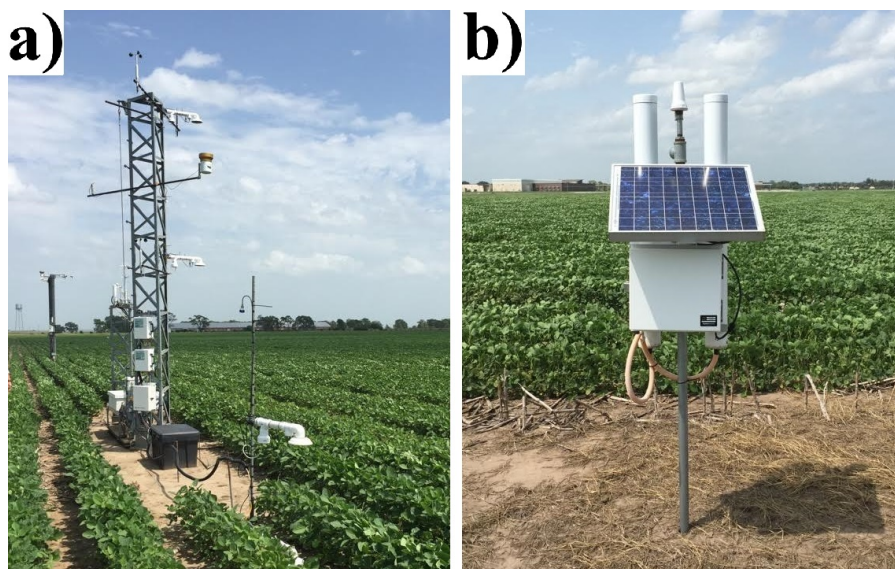
607

608

609

610

Figure 1. Study site (Mead Rainfed/US-Ne3) location in Nebraska (a) and locations of Eddy-Covariance Tower (EC), Cosmic-Ray Neutron Probe (CRNP) and Theta Probes (TPs) at the study site, 2014 (b).

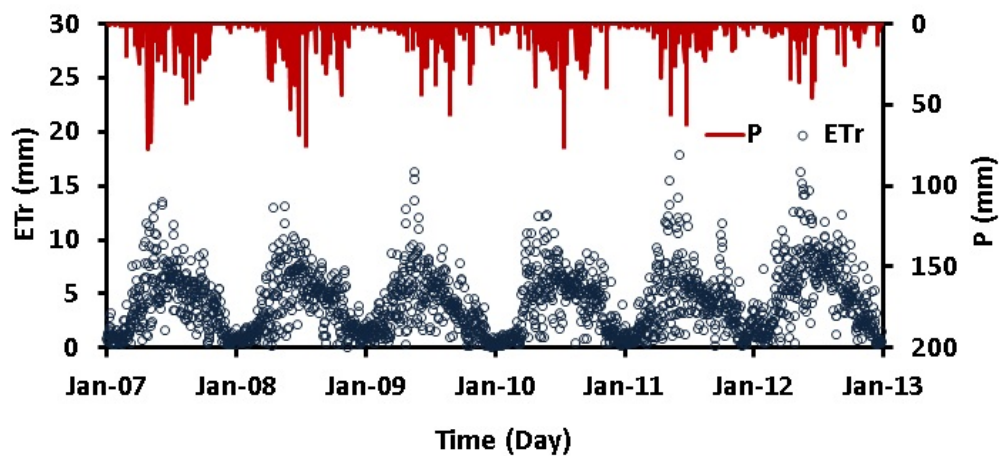


611

612

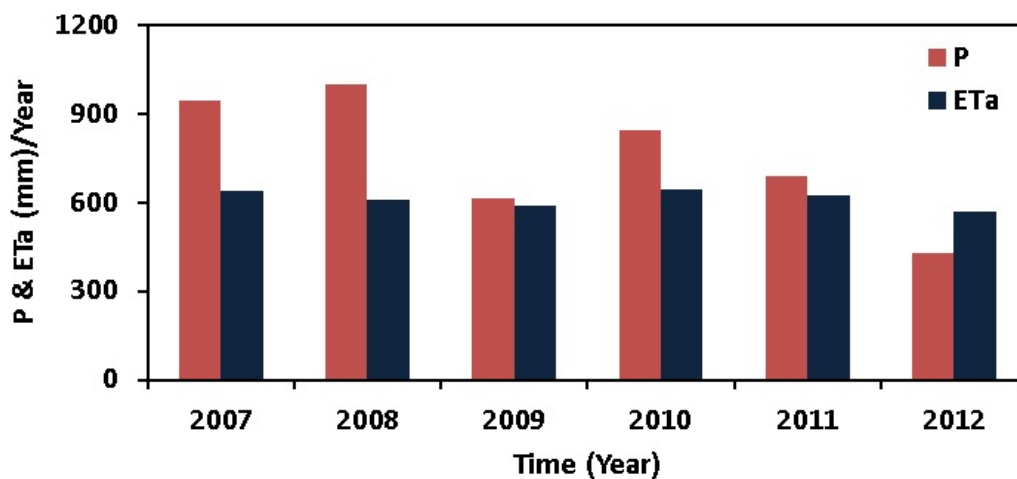
613

Figure 2. Eddy-Covariance Tower (a) and Cosmic-Ray Neutron Probe (b) Located at the Mead Rainfed (US-Ne3) Site.



614
615
616

Figure 3. Daily precipitation (P) and reference evapotranspiration (ET_r) during the calibration (2008–2010) and validation (2011–2012) periods at the Mead Rainfed (US-Ne3) Site.



617

618 Figure 4. Annual precipitation (P) and annual actual evapotranspiration (ET_a) at the Mead Rainfed
619 (US-Ne3) Site.

620

621

622

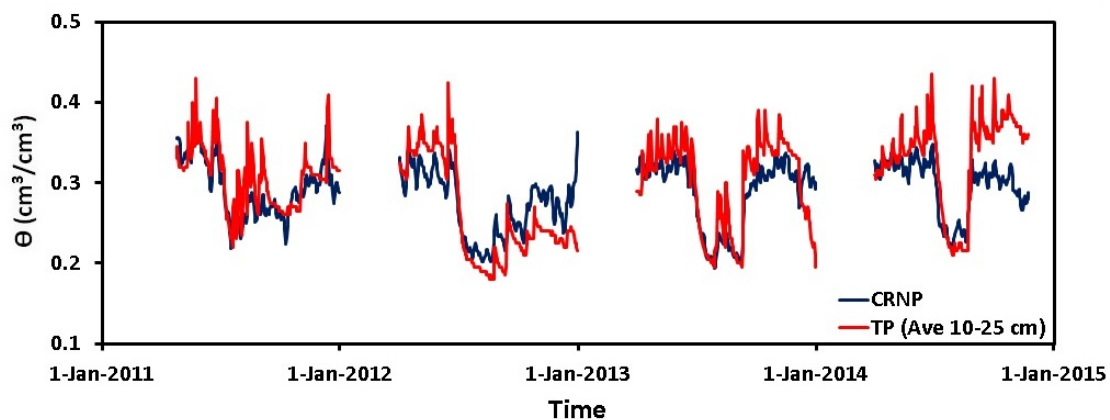
623

624

625

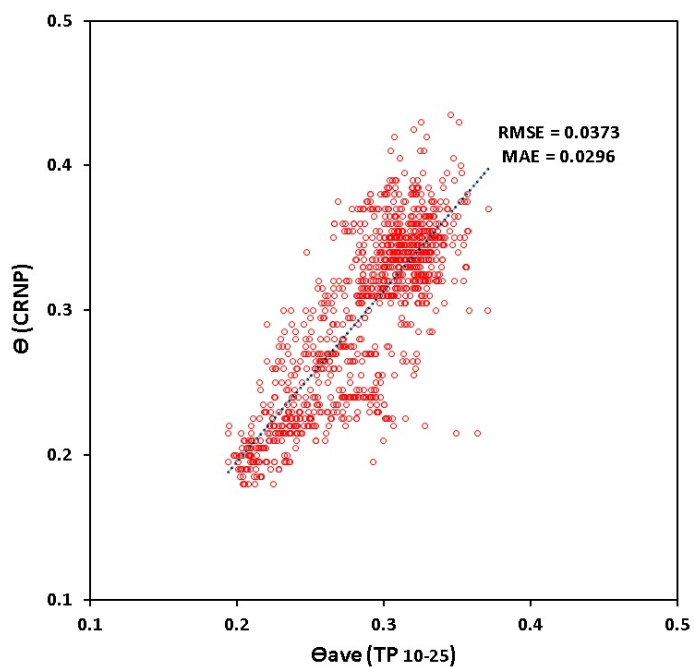
626

627



628
629
630
631
632
633
634
635
636

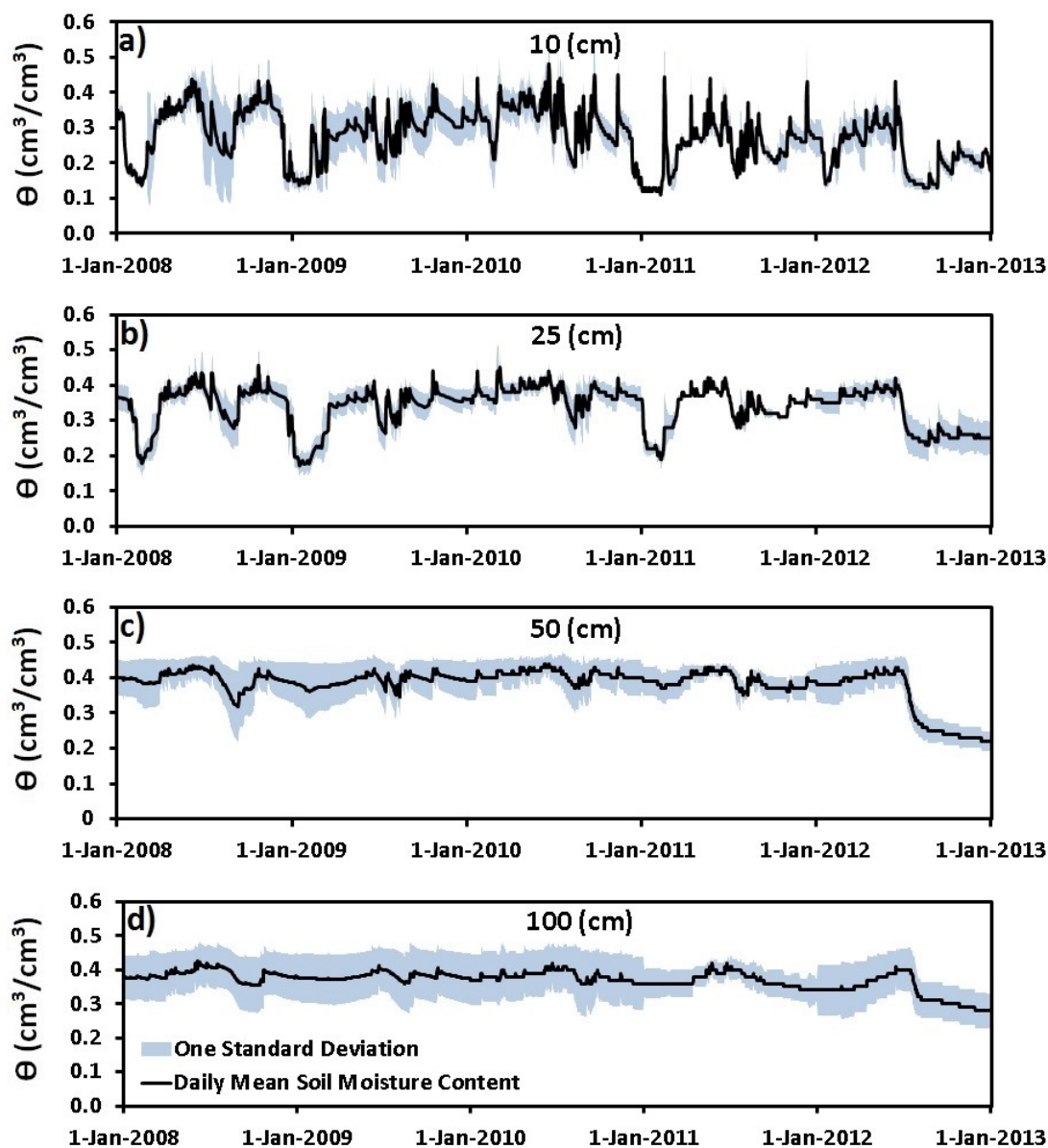
Figure 5. Time series of daily CRNP and spatial average TP *SWC* (θ) data.



637

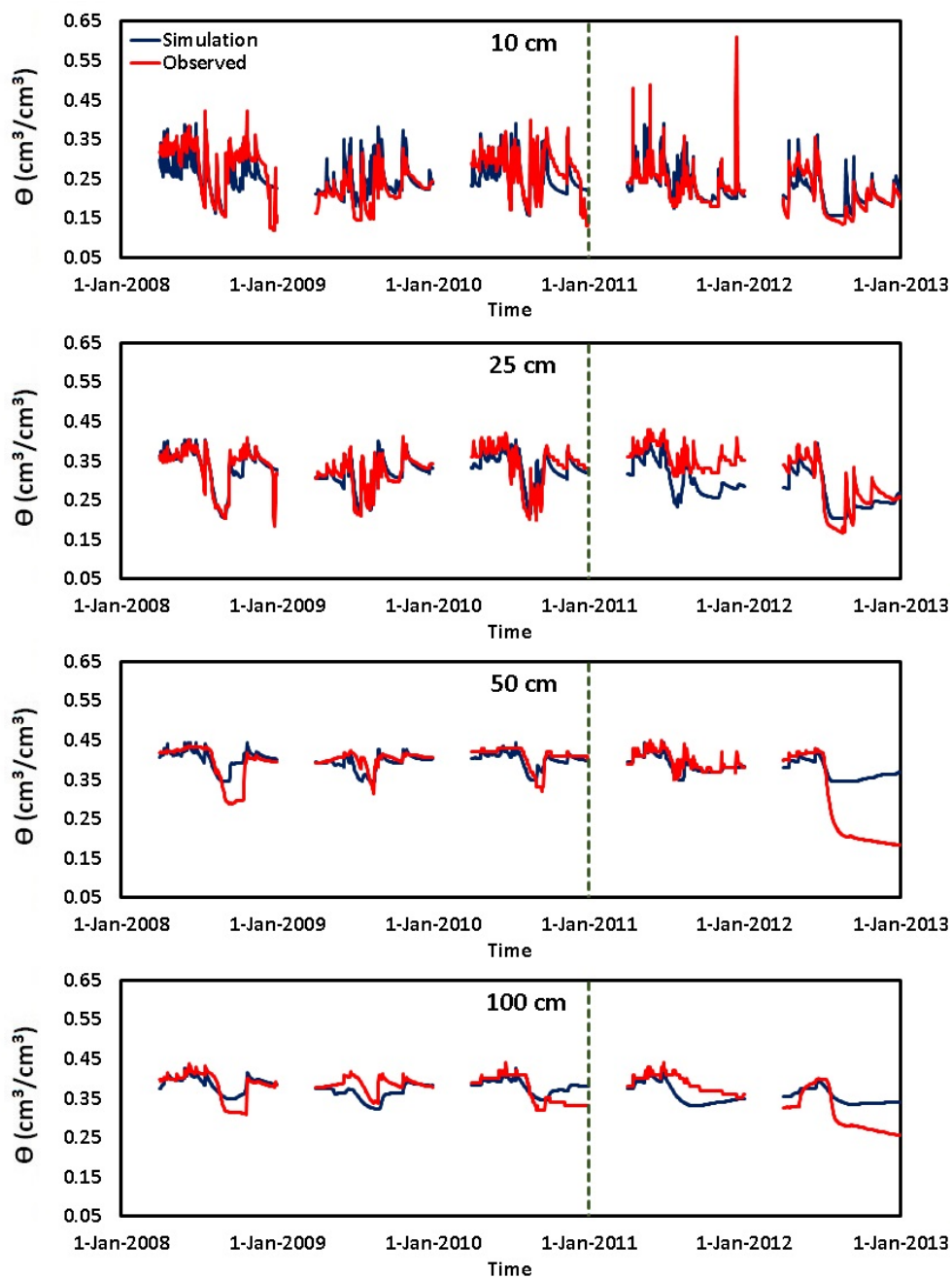
638

Figure 6. Comparison between daily CRNP and spatial average TP *SWC* (θ) data.



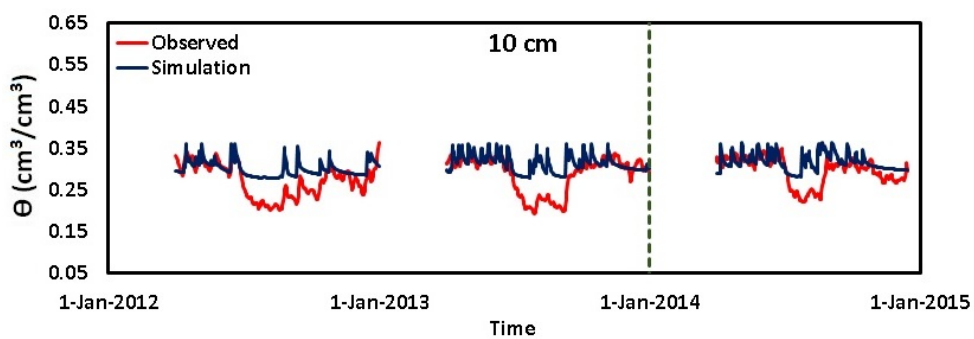
639

640 Figure 7. Temporal evolution of daily *SWC* (θ) at different soil depths. The black lines represent
641 daily mean *SWC* (θ) calculated from TPs in 4 different locations at study site and the blue areas
642 indicate one standard deviation.



643

644 Figure 8. Daily observed and simulated *SWC* (θ) during the calibration (2008–2010) and validation
645 (2011–2012) periods at TP 1 location.



646

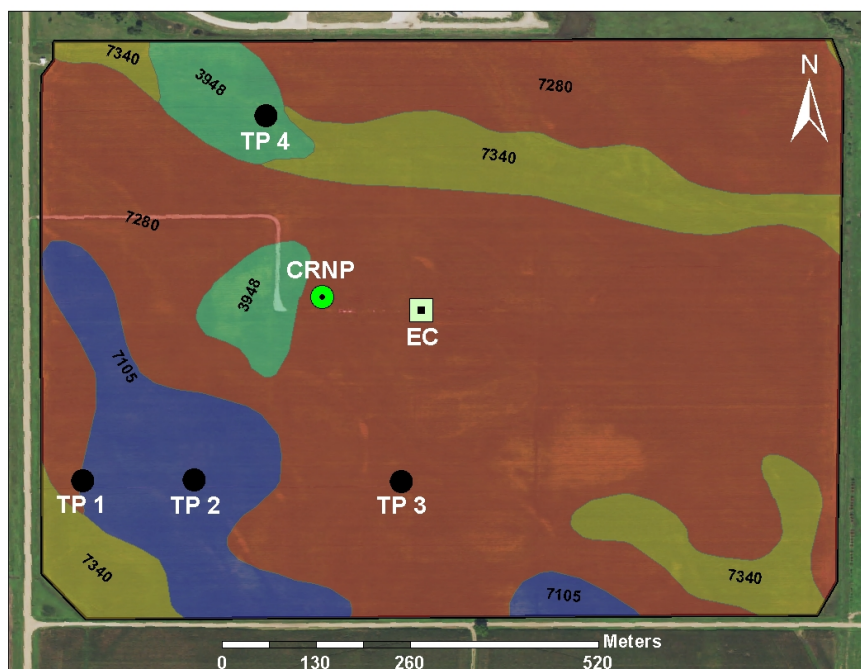
647 Figure 9. Daily observed and simulated *SWC* (θ) during the calibration (2012–2013) and validation
648 (2014) periods at the location of Cosmic-Ray Neutron probe.

649

650

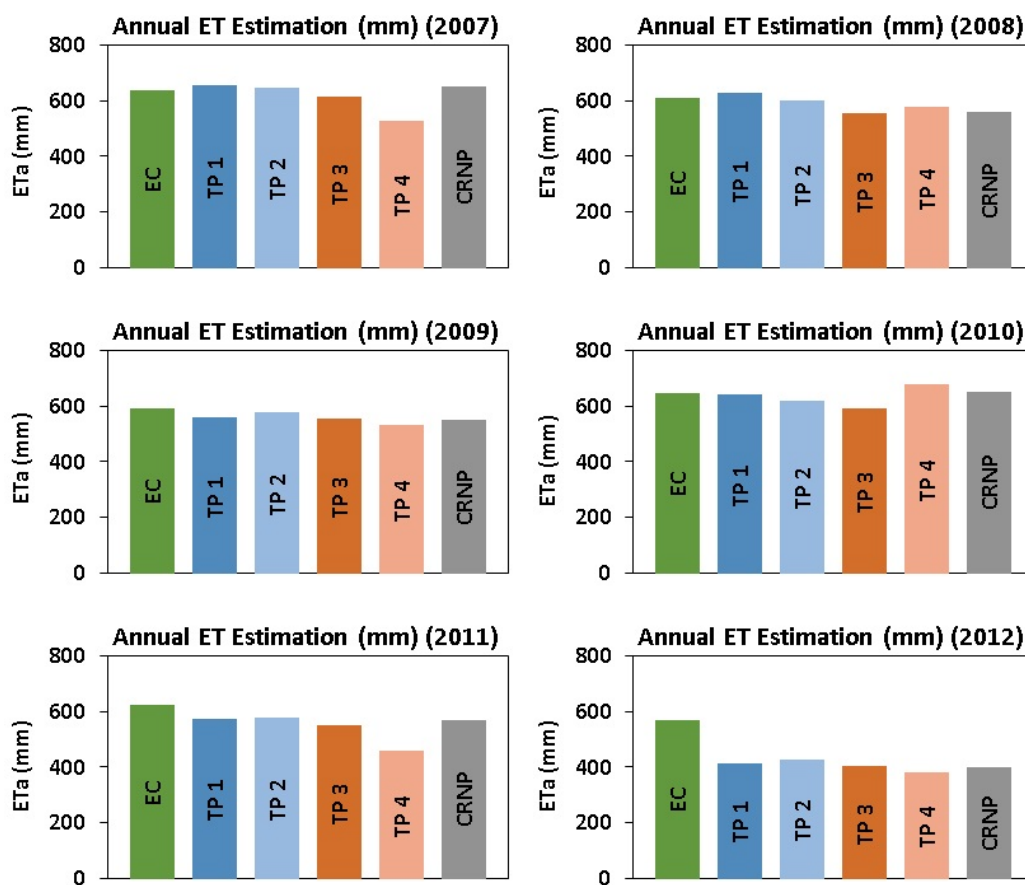
651

652



653

654 Figure 10. Variability of soil texture in the study field based on Web Soil Survey data (available at
655 <http://websoilsurvey.sc.egov.usda.gov/App/HomePage.htm>).



656

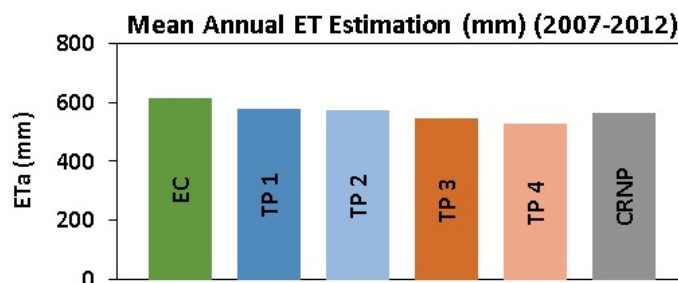
657 Figure 11. Annual actual Evapotranspiration (ET_a) estimation in different location at the study site
658 (2007-2012).

659

660

661

662

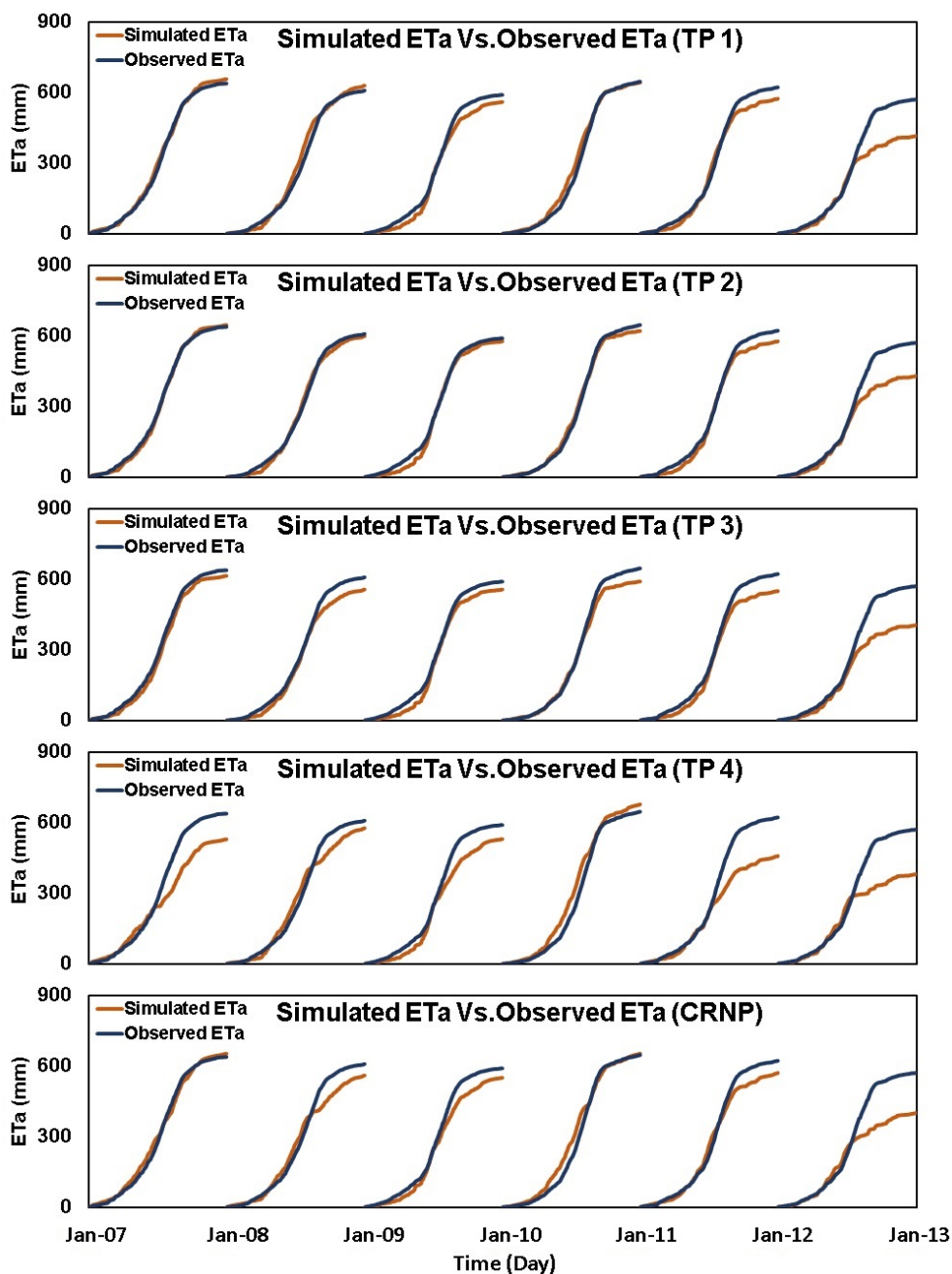


663

664

665

Figure 12. Mean Annual Actual Evapotranspiration (ET_a) estimation in different location at the study site (2007-2012).



666

667

668

Figure 13. Cumulative simulated actual *ET* versus cumulative observed actual *ET* in different locations at the study site (2007-2012).



669 **List of Tables**

670 Table 1. Bounds of the van Genuchten parameters used for inverse modeling.

671 Table 2. Goodness-of-fit measures for simulated and observed *SWC* data at different depths during
672 the calibration period (2008 to 2010) and validation period (2011-2012) at TPs locations.

673 Table 3. Goodness-of-fit measures for simulated and observed *SWC* data during the calibration
674 period (2012 to 2013) and validation period (2014) at CRNP location.

675 Table 4. Optimized van Genuchten parameters in different locations at the study site.

676 Table 5. Variability of soil texture in the study field based on Web Soil Survey data
677 (<http://websoilsurvey.sc.egov.usda.gov/App/HomePage.htm>).

678 Table 6. Goodness-of-fit measures for simulated and observed daily ET_a during the simulation
679 period (2007-2012) at study site.

680 Table 7. Summary of simulated yearly and average actual evapotranspiration (ET_a) (mm) and
681 observed yearly and average actual evapotranspiration (ET_a) (mm) from Eddy-Covariance
682 tower during 2007 to 2012.

683

684

685

686

687

688

689

690

691



692

Table 1. Bounds of the van Genuchten parameters used for inverse modeling.

Soil Parameter	θ_r (-)	θ_s (-)	α (1/cm)	n (-)	K_s (cm/day)	L (-)
Range	0.03–0.30	0.3–0.6	0.001–0.200	1.01–6.00	1–200	-1–1

693

694

695

696

697

698

699

700

701

702

703

704

705

706

707



708 Table 2. Goodness-of-fit measures for simulated and observed *SWC* data at different depths during
709 the calibration period (2008 to 2010) and validation period (2011-2012) at TPs locations.

Location	Depth (cm)	Calibration Period (2008-2010)				Validation Period (2011-2012)			
		R ²	MAE	RMSE	NSE	R ²	MAE	RMSE	NSE
TP 1	10	0.542	0.024	0.036	0.533	0.532	0.016	0.033	0.503
	25	0.742	0.014	0.022	0.739	0.716	0.029	0.040	0.486
	50	0.409	0.013	0.023	0.407	0.603	0.041	0.074	0.157
	100	0.352	0.015	0.022	0.343	0.419	0.027	0.038	0.358
TP 2	10	0.330	0.044	0.066	0.305	0.287	0.047	0.061	0.052
	25	0.623	0.010	0.020	0.604	0.718	0.038	0.055	0.135
	50	0.551	0.015	0.026	0.074	0.683	0.040	0.055	0.202
	100	0.424	0.019	0.027	-2.055	0.344	0.048	0.073	-0.473
TP 3	10	0.269	0.034	0.051	0.256	0.534	0.086	0.102	-4.265
	25	0.512	0.011	0.017	0.509	0.852	0.010	0.015	0.793
	50	0.549	0.015	0.023	-0.214	0.658	0.022	0.033	0.652
	100	0.238	0.018	0.029	-3.156	0.669	0.018	0.025	0.178
TP 4	10	0.412	0.029	0.044	0.406	0.580	0.051	0.071	-0.116
	25	0.434	0.016	0.025	0.350	0.594	0.029	0.042	0.490
	50	0.151	0.009	0.015	-13.400	0.443	0.041	0.073	0.036
	100	0.001	0.013	0.021	-12.058	0.292	0.026	0.039	0.238

710

711

712

713



714 Table 3. Goodness-of-fit measures for simulated and observed *SWC* data during the calibration
715 period (2012 to 2013) and validation period (2014) at CRNP location.

Location	Depth (cm)	Calibration Period (2012-2013)				Validation Period (2014)			
		R ²	MAE	RMSE	NSE	R ²	MAE	RMSE	NSE
CRNP	10	0.352	0.024	0.038	-0.059	0.083	0.021	0.034	-0.454

716

717

718

719

720

721

722

723

724

725

726

727

728

729



730

Table 4. Optimized van Genuchten parameters in different locations at the study site.

Location	Depth (cm)	θ_r (-)	θ_s (-)	α (1/cm)	n (-)	K_s (cm/day)	L (-)
TP 1	0-15	0.134	0.423	0.027	1.475	8.119	0.546
	15-35	0.136	0.408	0.007	1.345	11.540	0.480
	35-75	0.191	0.448	0.024	1.097	8.057	0.285
	75-175	0.071	0.430	0.025	1.069	9.807	0.364
TP 2	0-15	0.211	0.446	0.027	1.567	8.120	1.000
	15-35	0.197	0.434	0.006	1.191	8.655	0.022
	35-75	0.110	0.424	0.015	1.239	4.605	0.723
	75-175	0.109	0.408	0.020	1.302	6.780	0.000
TP 3	0-15	0.281	0.464	0.035	1.487	7.096	0.400
	15-35	0.072	0.402	0.012	1.085	29.960	0.353
	35-75	0.081	0.498	0.037	1.128	24.440	0.527
	75-175	0.085	0.500	0.039	1.147	17.540	0.496
TP 4	0-15	0.082	0.481	0.034	1.172	7.773	0.953
	15-35	0.200	0.426	0.013	1.217	14.060	0.044
	35-75	0.250	0.477	0.009	1.079	1.045	0.353
	75-175	0.200	0.487	0.012	1.070	1.454	0.985
CRNP	0-15	0.102	0.369	0.019	1.075	6.450	0.555

731



732
 733

Table 5. Variability of soil texture in the study field based on Web Soil Survey data
 (<http://websoilsurvey.sc.egov.usda.gov/App/HomePage.htm>).

Map Unit Symbol	Map Unit Name	Clay (%)	Silt (%)	Sand (%)	Hectors in Field	Percent of Field
3948	Fillmore silt loam, terrace, occasionally ponded	41.7	51.0	7.3	3.24	4.9%
7105	Yutan silty clay loam, terrace, 2 to 6 percent slopes, eroded	25.8	59.4	14.8	6.88	10.3%
7280	Tomek silt loam, 0 to 2 percent slopes	32.3	61.6	6.1	47.23	70.8%
7340	Filbert silt loam, 0 to 1 percent slopes	41.4	51.7	6.9	9.34	14.0%
Total Area of Field					66.69	100.0%

734
 735
 736
 737
 738
 739
 740
 741
 742
 743



744 Table 6. Goodness-of-fit measures for simulated and observed daily ET_a during the simulation
745 period (2007-2012) at study site.

Location	R^2	MAE	RMSE	NSE
TP 1	0.652	0.696	1.062	0.618
TP 2	0.754	0.610	0.907	0.746
TP 3	0.751	0.601	0.904	0.728
TP 4	0.413	0.878	1.387	0.168
CRNP	0.499	0.787	1.259	0.349

746

747

748

749

750

751

752

753

754

755

756

757

758

759



760 Table 7. Summary of simulated yearly and average actual evapotranspiration (ET_a) (mm) and
761 observed yearly and average actual evapotranspiration (ET_a) (mm) from Eddy-Covariance
762 tower during 2007 to 2012.

Location	Year						
	2007	2008	2009	2010	2011	2012	Average
EC	656.8	608.4	589.7	646.1	622.2	570.1	612.5
TP 1	646.1	629.0	559.8	642.1	573.9	415.5	579.5
TP 2	614.3	598.4	576.7	620.5	576.9	429.5	574.7
TP 3	529.0	556.1	556.4	590.4	549.8	405.2	545.4
TP 4	652.2	576.1	529.9	677.3	458.2	381.2	525.3
CRNP	656.8	559.6	549.9	652.8	570.7	400.1	564.2

763